Hindawi
Advances in Civil Engineering
Volume 2020, Article ID 3241602, 15 pages
https://doi.org/10.1155/2020/3241602

Research Article

The Horizontal Bearing Capacity of Composite Concrete-Filled Steel Tube Piles

Yunxiu Dong,[1,2] **Zhongju Feng**,[1] **Haibo Hu**,[1] **Jingbin He**,[1] **Qilang Zhang**,[3] **and Fuchun Wang**[1]

[1]*Highway School, Chang'an University, Xi'an, Shaanxi 710064, China*
[2]*School of Civil Engineering, Longdong University, Qingyang, Gansu 745000, China*
[3]*Guangdong Nanyue Transportation Investment & Construction Co. Ltd., Guangzhou, Guangdong 510000, China*

Correspondence should be addressed to Yunxiu Dong; dongyunxiu_0524@163.com

Received 31 July 2019; Revised 30 November 2019; Accepted 19 December 2019; Published 9 January 2020

Academic Editor: Chun-Qing Li

Steel casings (SCs) are extensively and increasingly used to stabilize the borehole wall in the construction of bridge pile foundations. Steel casings (SCs), together with reinforced concrete piles (RCPs), form composite concrete-filled steel tube piles (CCFSTPs), which differ significantly from ordinary RCPs in horizontal bearing capacity. In this study, based on the characteristics of CCFSTPs, the horizontal bearing capacity of a CCFSTP was examined through a centrifugal model test with the length of the steel casing (L_{SC}) and the modulus of the soil mass in the steel casing soil compaction zone (E_{SCSC_zone}) as variables. Pile-side soil resistance, load-displacement curves, and pile moment curves were obtained for the CCFSTP. The results show that increasing L_{SC} within a range of 12 cm significantly increases the ultimate horizontal bearing capacity of the CCFSTP, and further increasing L_{SC} beyond 12 cm produces a continuous increase in the ultimate horizontal bearing capacity of the CCFSTP but only to an insignificant extent. In addition, increasing E_{SCSC_zone} increases the ultimate horizontal bearing capacity of the CCFSTP, but to a relatively small extent. The results of this study provide a theoretical basis and technical support for the design and construction of CCFSTPs.

1. Introduction

Pile foundation [1–10] is an important part of highway bridge construction. In the construction of cast-in-place bored piles, the steel casing is usually used to stabilize the borehole wall or solve the slurry leakage problem of huge caves. When the steel casing is recycled, they are called reinforced concrete piles (RCPs). However, steel casings (SCs) used during construction are difficult to be recycled after piles are built due to subsequent construction requirements and their relatively large buried depth. Thus, together with reinforced concrete (RC), the SC form a concrete-filled steel tube composite structure, which is called composite concrete-filled steel tube (CFST) piles (CCFSTPs) in this study. Moreover, CCFSTPs have a large cross-section at the top and a small cross-section at the bottom, as shown in the Figure 1. The bearing capacity of a CCFSTP has a greater safety margin than that of an ordinary RCP of the same diameter. In fact, CCFSTPs have already been widely used in the construction of highway bridges. However, SC is basically considered to be a safety margin for the pile foundation. The preservation of this safety margin needs to be considered in design technique.

Scholars worldwide have conducted research relevant to composite CFST structures. The technical specification for CFST structures of China issued in 2014 mainly introduces design methods for circular CFSTs. This specification uses confinement theory and assumes that an increase in core concrete strength is directly proportional to the horizontal pressure provided by the outer steel tube [11]. Several countries, including the U.S. and Japan, have conducted research relevant to the use of CFST structures to build foundations. The American Institute of Steel Construction's Load and Resistance Factor Design Specification stipulates

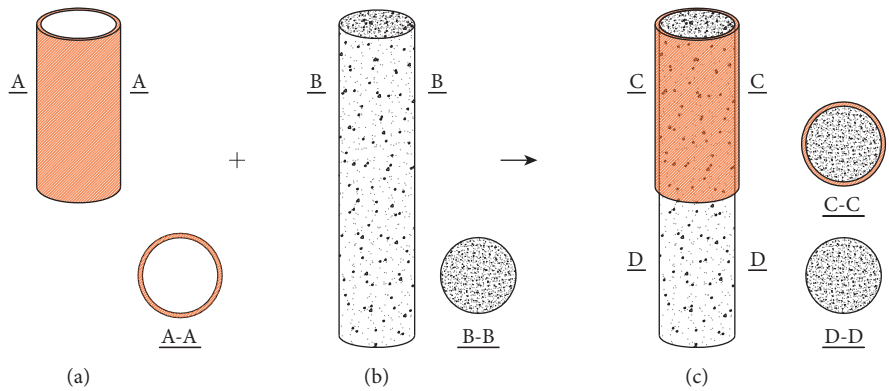

Figure 1: Composition of CCFSTP. (a) Steel casing (SC). (b) Reinforced concrete pile (RCP). (c) Composite concrete-filled steel tube pile (CCFSTP).

design methods for composite columns. This specification considers the overall stability of members under axial compression by treating CFST members as pure steel members and incorporating the strength of the concrete into that of the steel [12]. The Architectural Institute of Japan's concrete-filled steel tube (CFST) specification considers the confining effects of the steel tube on the core concrete when calculating the bearing capacity of a circular CFST member [13]. The British Standards Institute's Steel, Concrete, and Composite Bridge Specification for design of concrete bridges states that the core concrete is three-way compressed under the constraint of a steel pipe and the strength is increased when calculating the bearing capacity of a circular CFST member [14]. European Standardization Committee's Eurocode 4 Design of steel and for buildings pointed out that the design of the steel concrete composite structure is superimposed on the full plastic section, and then the bearing capacity is corrected by comparison and analysis of the test [15]. Johansson et al. [16] studied the mechanical behaviors of 13 CFST column specimens under three different loading conditions through a static test and found that the bond strength greatly affected the confinement effects when the load was applied only to the concrete part and thus affects mechanical properties of the columns. Trentadue et al. [17] proposes closed-form approximations of the axial force-bending moment interaction diagrams for reinforced concrete columns and concrete-filled steel tubes with circular cross-section. Yousuf et al. [18] studied the behavior of hollow and concrete-filled stainless steel tubular columns under static and impact loading. Patel et al. [19, 20] described verification and applications of a multiscale model for CFST columns. Brown et al. [21], Aguirre et al. [22], and Montejo et al. [23] studied the nonlinear seismic behavior of reinforced concrete-filled steel tubes. Jung et al. [24] improved shear design equations through further experimental and analytical research on shear resistance and behavior of circular CFT. Du et al. [25] and Ding et al. [26] investigated the failure modes, the impact force time history curves, and the strain time history curves to evaluate the behavior of the CFCST member under an impact load. Zhu et al. [27] and Wang et al. [28] studied the factors influencing the bearing capacity of concrete-filled steel tube columns. All of the aforementioned studies focus on the mechanical properties and bearing capacity of composite steel tube-concrete structures. However, there is a lack of research on the horizontal bearing capacity of CCFSTPs when they interact with the surrounding rock and soil mass. The functional difference between bridge pile foundations and CFST columns results in a difference in the horizontal bearing capacity between CCFSTPs and CFST columns. Therefore, it is necessary to study the horizontal bearing capacity of CCFSTPs.

In this study, based on the centrifugal model test, the horizontal bearing capacity of a CCFSTP affected by the length of the steel casing (L_{SC}) and the elastic modulus of the soil mass in the steel-casing soil compaction (SCSC) zone (E_{SCSC_zone}) are examined. The load transfer mechanism for the CCFSTP under horizontal loading is analyzed, with the aim of providing a technical basis for the design and construction of bridge pile foundations.

2. Experimental Investigation

In order to study the horizontal bearing capacity of the piles, a series of centrifugal model tests were carried out to analyze the effect of steel casing and soil modulus in the steel casing soil compaction zone on the bearing capacity of the piles.

2.1. Physical Model. In order to study the difference in horizontal bearing capacity between composite concrete-filled steel tube piles (CCFSTPs) and ordinary reinforced concrete pile (RCP), 4 model CCFSTPs and 1 model RCP were designed, as shown in Table 1 and Figure 2, taking into account the influence of steel casing length. The piles are friction piles.

The ground in the model is composed of 40 cm thick noncollapsible loess. In practice, the steel casing has a compaction effect on the soil around the pile. To truly reflect the mechanical conditions of the original CCFSTP, the soil compaction effects of the steel casing on the horizontal bearing capacity of the CCFSTP were simulated in the model test by altering E_{SCSC_zone} (the SCSC zone is a zone with a thickness of 15 mm around the steel casing, where 15 mm is

Table 1: Size of model piles.

Model pile number	L (cm)	L_{SC} (cm)	D (mm)	D_{SC} (mm)	t (mm)	t_{SC} (mm)
CCFSTP-1	35	20	25	30	2	2
CCFSTP-2	35	16	25	30	2	2
CCFSTP-3	35	12	25	30	2	2
CCFSTP-4	35	8	25	30	2	2
RCP-0	35	0	25	0	2	2

Note. L represents the length of the model pile. L_{SC} represents the length of the steel casing. D represents the outside diameter of the model pile. D_{SC} represents the outside diameter of the steel casing. t represents the thickness of the model pile. t_{SC} represents the thickness of the steel casing.

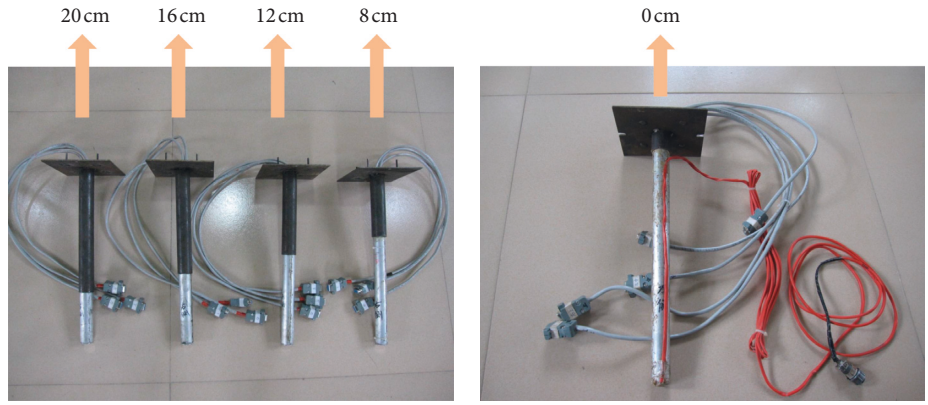

Figure 2: Photograph of the model piles. (a) Composite concrete-filled steel tube piles with different steel casing length. (b) Conventional reinforced concrete pile without steel casing.

the radius of the steel casing). Due to the difficulty of operating within the limited space inside the model chamber, a soil compaction mould designed in-house was used to prepare the foundation soil in the SCSC zone in advance [26], as shown in Figure 3.

In this paper, steel casing length L_{SC} and E_{SCSC_zone} were selected as the variables. Table 2 summarizes the test conditions.

2.2. Material Properties. Because cast-in-situ piles are composed of reinforced concrete, it is difficult to form the same strength of concrete as the prototype piles as soon as possible. Therefore, similar materials will be used for simulation according to the recognition criteria. The model material is controlled by the bending stiffness EI (elastic modulus and moment of inertia), as shown in equation (1). In this study, aluminum pipe was used as material for the ordinary reinforced concrete pile. Table 2 shows the characteristics of test piles. Because Young's modulus of the prototype pile is 18.7 GPa, the similarity rate of 100 is available according to equation (1) and Table 3:

$$n^4 E_m I_m = E_p I_p = \frac{n^4 E_m \pi \left(D_m^4 - d_m^4\right)}{64} = \frac{E_p \pi D_p^4}{64}, \quad (1)$$

where E_m is Young's modulus of the model; E_p is Young's modulus of the prototype; I_m is inertia moment of the model; I_p is inertia moment of the prototype; n is the similarity rate; D_m is outer diameter of the model; d_m is inner diameter of the model; D_p is diameter of the prototype.

Four model piles of composite concrete-filled steel tube piles have the same materials with the ordinary reinforced concrete pile. The steel casing was simulated by a steel pipe. Table 4 shows the characteristics of the steel casing.

The main physical properties of the noncollapsible loess were tested by a consolidation test (Figure 4(a)), a moisture content test (Figure 4(b)), and a direct shear test (Figure 4(c)). Density was obtained according to the mass and volume of the soil. Compression modulus was obtained by the consolidation test. The moisture content was measured by the moisture content test. The internal friction angle and cohesive force were calculated by the direct shear test. The results are shown in Table 5.

2.3. Instrument of Experiments. In this study, TLJ-3 type geotechnical centrifuge at Chang'an University with an effective radius of rotation of 2 m was used, as shown in Figure 5. The maximum centrifugal acceleration is 200g. It has a container and a balancing container as a beam type of the centrifuge. The dimensions of the container are 700 mm in length, 500 mm in height, and 360 mm in width. There are 40 channels on the centrifuge, which could transmit the collected data to the computer. This study satisfied the similitude laws [29]. Detailed similitude ratios between the model and the prototype are shown in Table 6.

BE120-3AA strain gauges with a sensitivity factor of 2.0–2.2 and a resistance of 120 Ω were used to measure the strain of the piles. To ensure a relatively high survival

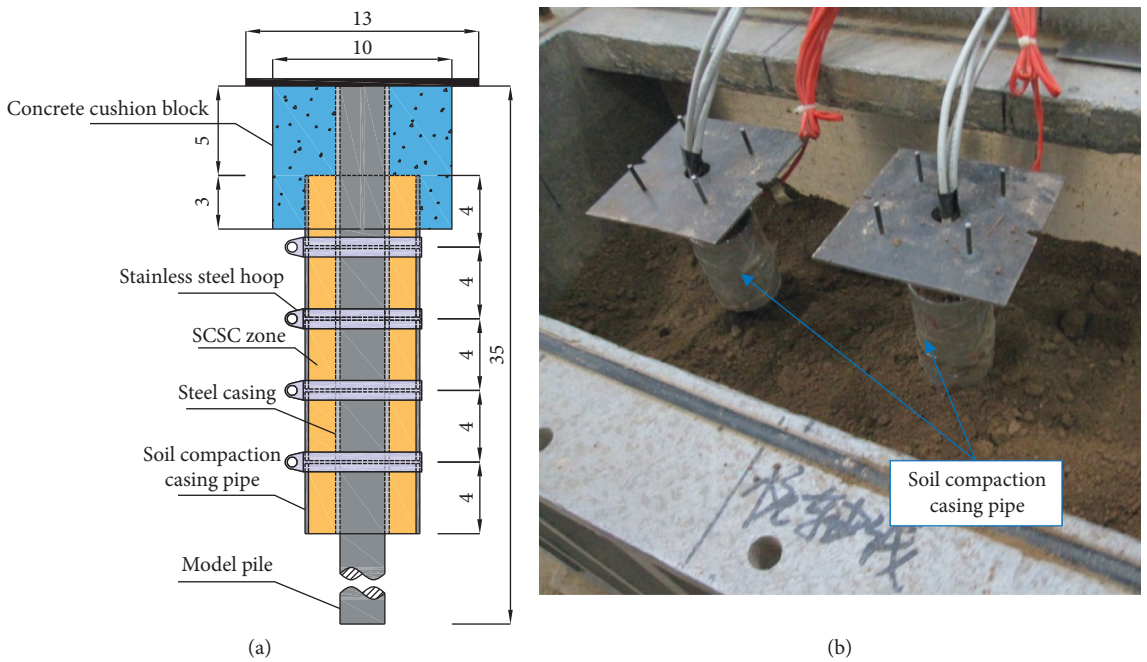

Figure 3: Schematic diagram of the soil compaction mould (unit: cm).

Table 2: Test conditions.

Name	Steel casing length L_{SC} (cm)	E_{SCSC_zone} (MPa)
RCP	0	$1.0E_{Non\text{-}SCSC\ zone}$
CCFSTPs	8, 12, 16, and 20	$1.1E_{Non\text{-}SCSC\_zone}$
	8	$1.1E_{Non\text{-}SCSC\_zone}$, $1.2E_{Non\text{-}SCSC\_zone}$, $1.3E_{Non\text{-}SCSC\_zone}$, $1.4E_{Non\text{-}SCSC\_zone}$, and $1.5E_{Non\text{-}SCSC\_zone}$

Note. "$E_{Non\text{-}SCSC\_zone}$" signifies the compressive modulus of the soil mass in the non-SCSC zone.

Table 3: Characteristics of test piles.

g level	Pile length L		Outside diameter D		Thickness t		Young's modulus E (GPa)
	Model (mm)	Prototype (m)	Model (mm)	Prototype (m)	Model (mm)	Prototype (m)	
100	350	35	25	2.5	2	0.2	40.2

Table 4: Characteristics of steel casing.

g level	Length L_{SC}		Outside diameter D		Thickness t		Young's modulus E (GPa)
	Model (cm)	Prototype (m)	Model (mm)	Prototype (m)	Model (mm)	Prototype (m)	
100	20	20	30	3	2	0.2	164
	16	16					
	12	12					
	8	8					

rate for the resistance strain gauges after being buried in the soil layer, the model piles were cut open lengthwise and six pairs of strain gauges were placed on opposite sides at a certain interval on the inner wall. After the strain gauges were affixed, the model piles were pasted and restored by epoxy resin and the position of the pile shaft strain gauges were laid out, as shown in Figure 6. Since the depth of the pile body into the soil layer is 30 cm and the pile length is 35 cm, the position of the first group of the strain gauge is 5 cm away from the pile top. The second group to the fifth group of the strain gauge are located according to the length of steel casing. To save the number of strain gauges and reflect the strain near the pile bottom, the sixth group of strain gauges is arranged 2 cm away from the pile bottom.

The aluminium pipes and steel pipes were bonded with epoxy resin, regardless of the friction between them. Finally, sandpaper was used to polish the outer surface of the model

(a) (b) (c)

Figure 4: Tests: (a) consolidation test; (b) moisture content test; (c) direct shear test.

Table 5: Physical properties of loess.

Name	Density ρ (g/cm^3)	Compressive modulus $E_{\text{Non-SCSC zone}}$ (MPa)	Moisture content ω (%)	Cohesion c (kPa)	Internal friction angle φ (°)
Loess	1.7	19.8	13.5	27	21

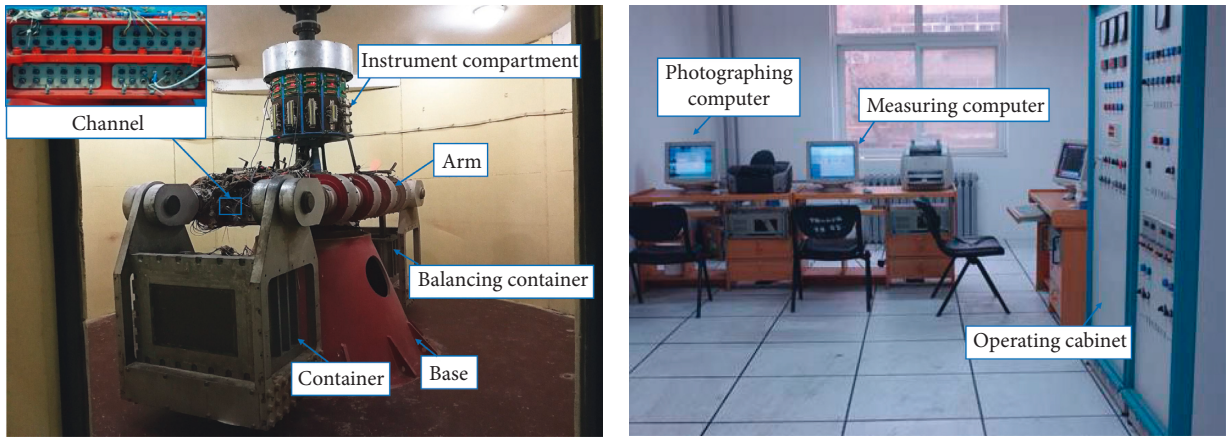

(a) (b)

Figure 5: TLJ-3 type geotechnical centrifugal.

Table 6: Similitude ratios in centrifugal model tests.

Parameter	Ratio
Length	$1:n$
Diameter	$1:n$
Displacement	$1:n$
Moment of inertia	$1:n^4$
Stress and strain	1:1
Force	$1:n^2$

Note. Centrifugal acceleration = $n{\cdot}g$.

pile to make its bearing characteristics more similar to the actual pile. BW11-1.2 string compression-type minisoil pressure cells (diameter: 12 mm; definition: 1 $\mu\varepsilon$; sensitivity factor: (0.25 ± 0.01) %; range: 0–1.2 MPa; accuracy: 0.001 MPa) were affixed to each pile at a certain interval to measure the pile-side soil resistance. Figure 3 shows the placement of the strain gauges and the soil pressure cells on the CCFSTP.

2.4. Test Procedure. The specific steps are as follows, and the main test procedures are shown in Figure 7.

(a) To ensure uniform density of the soil in the container, compress a certain mass of soil into a certain volume. In this test, the soil density is 1.7 g/cm^3 and each layer of soil is compressed to 2 cm. Since the container length is 70 cm and the width is 36 cm, each layer of soil is compressed to 5040 cm^3, so the soil quality required for each layer is 8568 g. First, weigh 8568 g of soil and put it into a plastic bag. Then, use a shovel to evenly spread the soil into the container. Finally, use a vibrator to compress the soil to 2 cm. Then, drill holes according to the pile position, as shown in Figure 8. The depth of the hole is 30 cm. The aperture was slightly smaller than the pile diameter, which makes the axial resistance between pile and soil closer to the actual value. Finally, the pile was pressed into the hole.

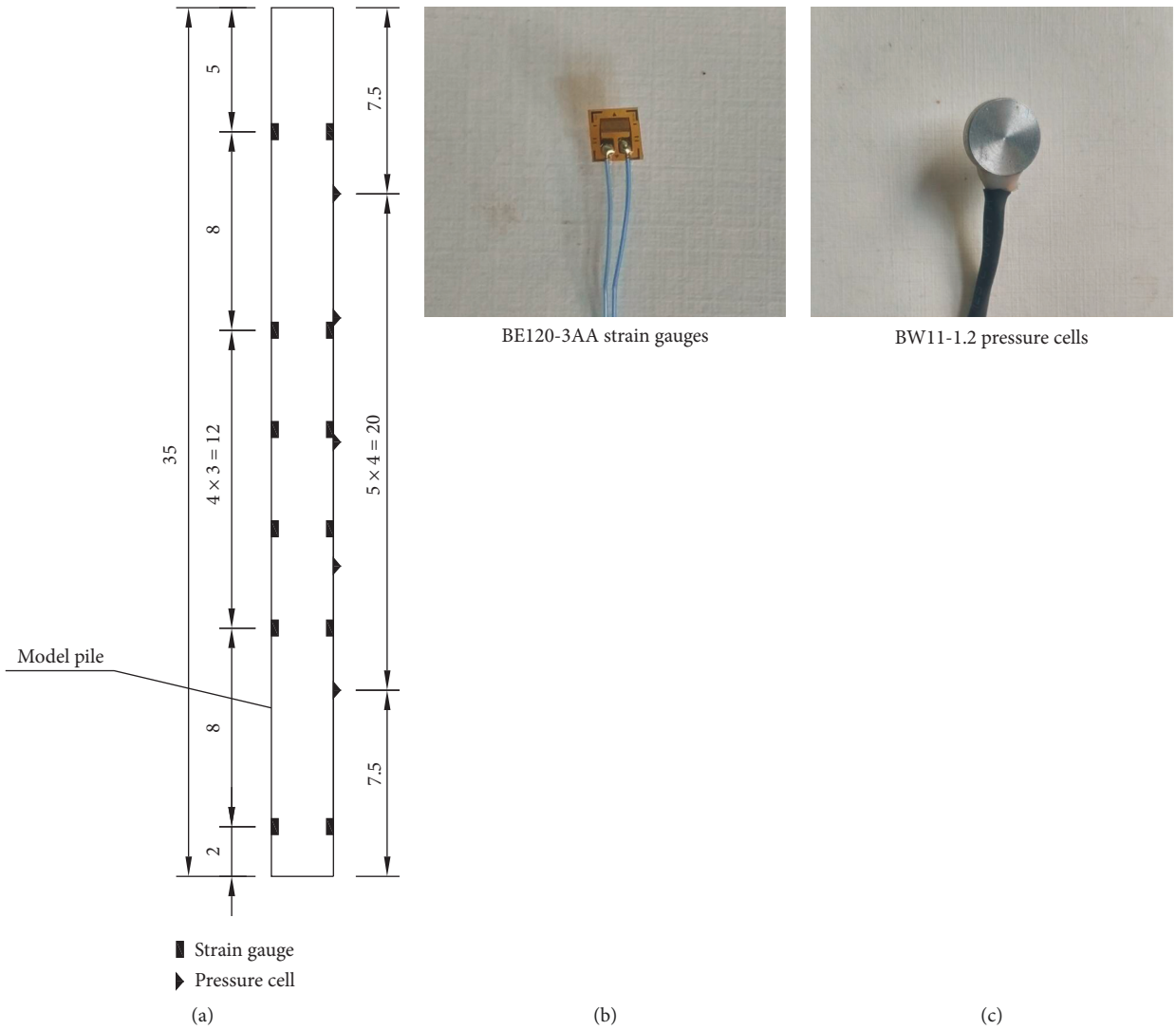

Figure 6: Placement of the strain gauges and the soil pressure cell (unit: cm).

(b) The container was put into the centrifuge.

(c) Firstly, the reaction frame was bolted to the container. Then, soil pressure cells, strain gauges, and the displacement gauges were connected to the centrifuge channel.

(d) 100 g level was conducted for five minutes.

(e) The data was transferred to the computer.

(f) Repeate the steps above when one load ends. Horizontal loading was achieved by adding steel plates to the loading platform (a hook at end of the strand), and the horizontal loading was divided into eight levels; the loading was 25 N, 50 N, 75 N, 100 N, 125 N, 150 N, 175 N, and 200 N, as shown in Figure 9.

3. Results and Discussion

3.1. CCFSTP Side Soil Resistance. Similar patterns can be observed for the variation in the pile-side soil resistance with L_{SC} under various horizontal loads. Here and later, the test condition with a horizontal load of 150 N is taken as an example for analysis. Figure 10 shows the variation patterns of the pile-side soil resistance with L_{SC}.

The pile-side soil resistance of the CCFSTP is lower than that of the ordinary RCP for the same depth, and the pile-side soil resistance gradually decreases as the steel casing length increases. For the CCFSTP, the pile-side soil resistance increases first and then decreases with increasing depth. The pile-side soil resistance approached zero at a depth of approximately 17 cm below the surface, and it increased as the depth increased further. This is likely to indicate that the CCFSTP underwent inflection deformation at a depth of approximately 17 cm below the surface. As the steel casing length increased, the maximum pile-side soil resistance of the CCFSTP gradually decreased. The maximum pile-side soil resistance of the CCFSTP is 125.3 kPa, 123.0 kPa, 120.5 kPa, and 118.1 kPa when steel casing length is 8 cm, 12 cm, 16 cm, and 20 cm, respectively, which are 10.9%, 12.6%, 14.4%, and 16.1% lower than that of the

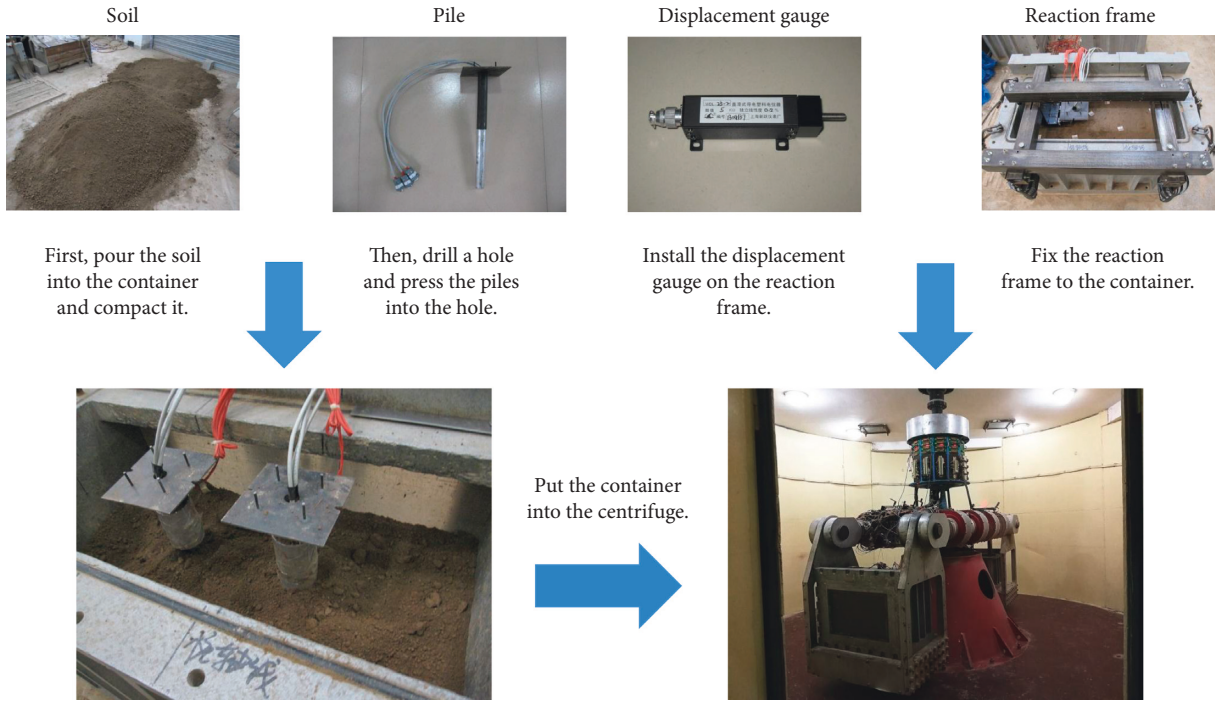

Figure 7: The main test procedures.

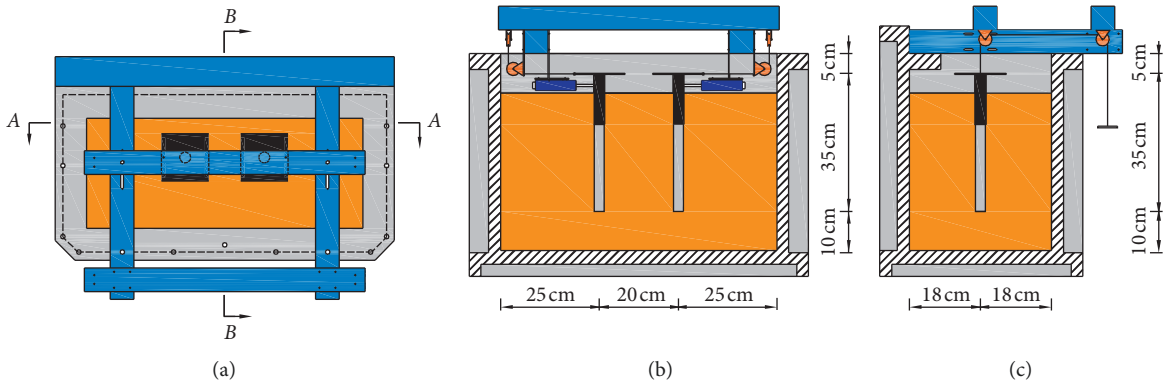

Figure 8: The position of the model piles: (a) Planar graph; (b) A-A section diagram; (c) B-B section diagram.

Adding round steel plates with holes to the hook at the end of the strand

Figure 9: Horizontal loading device.

ordinary RCP, respectively. This is because as the steel casing length increases, the stiffness of CCFSTP increases. Moreover, the diameter of the steel casing is slightly larger than the borehole size, which has extrusion effect on the soil, and with the increase of the length of the steel casing, the extrusion area of the steel casing and the soil increases and larger pile-side soil resistance can be obtained. Consequently, the depth of the soil mass on the side of the pile affected by the pile is increased, which lead to a decrease in the maximum pile-side soil resistance.

Figure 11 shows the variation patterns of the pile-side soil resistance with E_{SCSC_zone}.

As E_{SCSC_zone} values increases, the pile-side soil resistance of the CCFSTP increases. However, the pile-side soil resistance of the CCFSTP remains lower than that of the

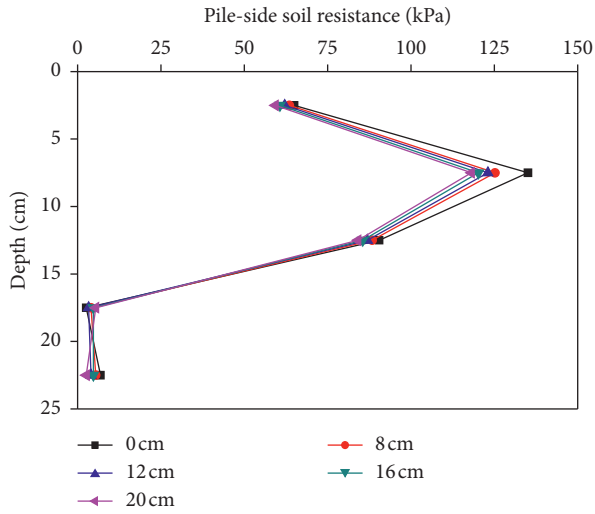

Figure 10: Change rule of the pile-side soil resistance with L_{SC}.

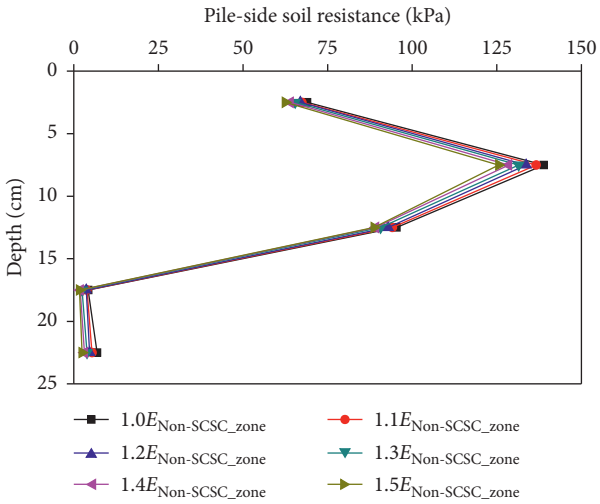

Figure 11: Change rule of the pile-side soil resistance with E_{SCSC_zone}.

ordinary RCP. The maximum soil resistances on the side of the CCFSTP were 118.1 kPa, 120.8 kPa, 123.7 kPa, 125.6 kPa, and 127.8 kPa when $E_{SCSC\_zone} = 1.1E_{Non\text{-}SCSC\_zone}$, $1.2E_{Non\text{-}SCSC\_zone}$, $1.3E_{Non\text{-}SCSC\_zone}$, $1.4E_{Non\text{-}SCSC\_zone}$, and $1.5E_{Non\text{-}SCSC\_zone}$, respectively, which are 16.1%, 14.1%, 12.1%, 10.7%, and 9.2% lower than that of the ordinary RCP, respectively. This is because as the modulus of soil mass in the steel casing soil compaction zone increases, the soil mass around the CCFSTP becomes denser and the area of the soil around of the pile affected by the pile decreases, resulting in an increase in the maximum pile-side soil resistance.

3.2. Horizontal Bearing Capacity of the CCFSTP. Figure 12 shows the load-displacement curves and load-displacement gradient curves of the CCFSTP under various values of L_{SC}.

As demonstrated in Figure 12, under the same horizontal displacement, the longer the length of the steel casing, the greater the load the pile can bear. The load-displacement gradient curves of the CCFSTP under various L_{SC} values contain no notable inflection points, indicating that the pile has not been damaged. As a result, the ultimate bearing capacity of the pile cannot be determined based on the inflection points of the curves. In this paper, the ultimate horizontal bearing capacity of the CCFSTP is controlled by displacement. The horizontal load corresponding to when the CCFSTP underwent a horizontal displacement of 0.4 mm is used as its ultimate bearing capacity [30]. Let α_H be the degree of impact on the ultimate horizontal bearing capacity of the pile. $\alpha_H = (H - H_0)/H_0 \times 100\%$, where H_0 is the ultimate horizontal bearing capacity of the ordinary reinforced concrete pile (RCP) and H is the ultimate horizontal bearing capacity of the CCFSTP. Figure 13 shows how the ultimate horizontal bearing capacity of the CCFSTP varies with the steel casing length.

As shown in Figure 13, the ultimate horizontal bearing capacity of the CCFSTP is higher than that of the ordinary RCP, and it increased as L_{SC} values increased. The ultimate horizontal bearing capacity of RCP ($L_{SC} = 0$ cm) is 69.5 N. The ultimate horizontal bearing capacity of the CCFSTP is 78.9 N, 83.7 N, 85.4 N, and 85.8 N when the steel casing length is 8 cm, 12 cm, 16 cm, and 20 cm, respectively. With the increase of steel casing length, the horizontal ultimate bearing capacity of CCFSTP increases gradually. The reason is that the diameter of the steel casing is slightly larger than the borehole size, which has extrusion effect on the soil, and with the increase of the length of the steel casing, the extrusion area of the steel casing and the soil increases and larger pile-side soil resistance can be obtained. The aforementioned analysis shows that the ultimate horizontal bearing capacity of the CCFSTP increased to a relatively large extent as the steel casing length increased within a range of 12 cm and that the ultimate horizontal bearing capacity of the CCFSTP continued to increase as the steel casing length increased beyond 12 cm, albeit to a relatively small extent. When the steel casing length is 8 cm, the ultimate bearing capacity is increased by 13.3%, indicating that the existence of steel casing can improve the ultimate bearing capacity. When the steel casing length is 16 cm, the increase of ultimate bearing capacity is 22.7%. It is only 2.5% higher than the CCFSTP with a steel casing length of 12 cm. This is because when the steel casing length exceeds a certain value, the increase of the steel casing length has little effect on the horizontal bearing capacity of the CCFSTP.

Figure 14 shows the load-displacement curves and the load-displacement gradient curves of the CCFSTP under various values of E_{SCSC_zone}.

As demonstrated in Figure 14, the load-displacement gradient curves of the CCFSTP under various values of E_{SCSC_zone} contain no notable inflection points, indicating that the pile has not been damaged. Similarly, the ultimate bearing capacity of the CCFSTP is also controlled by horizontal displacement. In addition, it can also be seen from Figure 14 that under the same horizontal displacement, the larger the modulus of soil mass in the steel casing soil compaction zone, the greater the load the pile can bear. Figure 15 shows the variation pattern of the ultimate

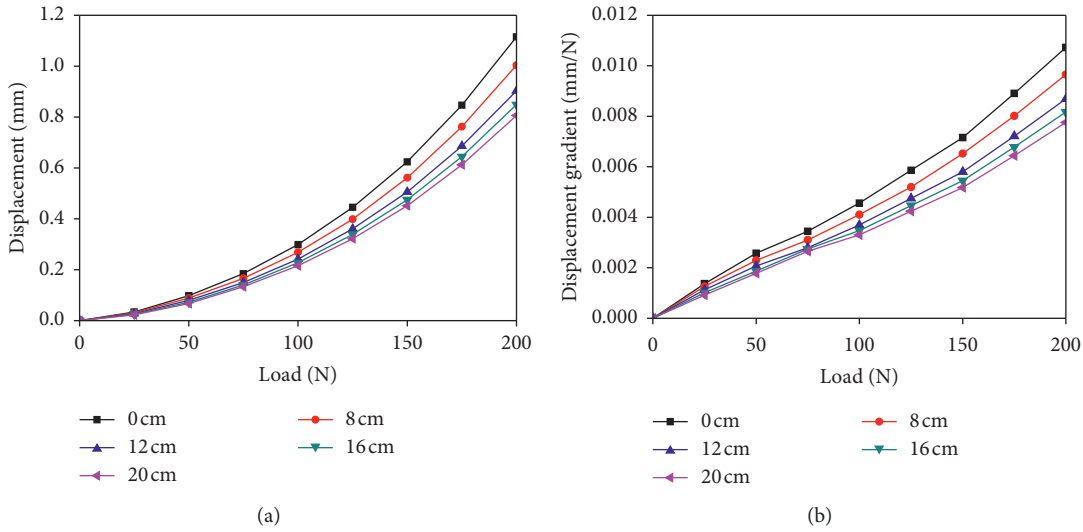

Figure 12: Load-displacement curves and load-displacement gradient curves of the CCFSTP under various L_{SC} values.

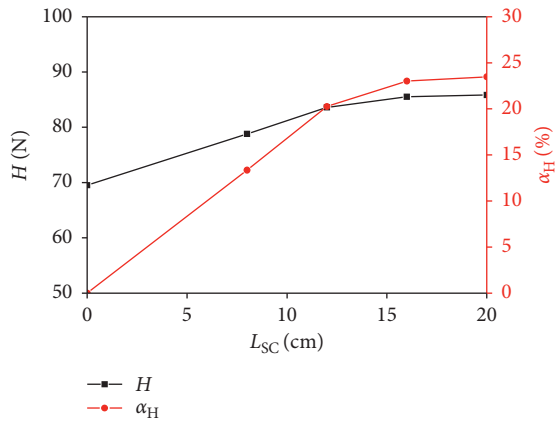

Figure 13: Effects of L_{SC} on the ultimate horizontal bearing capacity of the CCFSTP.

horizontal bearing capacity of the CCFSTP foundation with E_{SCSC_zone}.

As shown in Figure 15, the ultimate horizontal bearing capacity of the CCFSTP is higher than that of the ordinary RCP, and it increases as E_{SCSC_zone} values increases. The ultimate horizontal bearing capacity of RCP ($E_{SCSC\_zone} = 1.0E_{Non\text{-}SCSC\_zone}$) is 69.5 N. The ultimate horizontal bearing capacity of the CCFSTP is 78.9 N, 81.0 N, 82.8 N, 83.6 N, and 84.4 N when the E_{SCSC_zone} values is $1.1E_{Non\text{-}SCSC\_zone}$, $1.2E_{Non\text{-}SCSC\_zone}$, $1.3E_{Non\text{-}SCSC\_zone}$, $1.4E_{Non\text{-}SCSC\_zone}$, and $1.5E_{Non\text{-}SCSC\_zone}$, respectively. With the increase of modulus of soil mass in the steel casing soil compaction zone, the horizontal ultimate bearing capacity of CCFSTP increases gradually when the length of steel casing is constant. The main reason is that with the increase of modulus of soil mass in the zone which is around CCFSTP, the soil around CCFSTP is not easy to be compressed, and the pile-side soil resistance increases. It can be seen that the ultimate horizontal bearing capacity of the CCFSTP increased to a relatively large extent as E_{SCSC_zone} values increased within a range of $1.3E_{Non\text{-}SCSC\_zone}$ and that the ultimate horizontal bearing capacity of the CCFSTP continued to increase as the E_{SCSC_zone} values increased beyond $1.3E_{Non\text{-}SCSC\_zone}$, albeit to a relatively small extent. When the E_{SCSC_zone} value is $1.1E_{Non\text{-}SCSC\_zone}$, the ultimate bearing capacity is increased by 13.3%, indicating that the increase of soil modulus around the pile can improve the ultimate bearing capacity. When the E_{SCSC_zone} value is $1.4E_{Non\text{-}SCSC\_zone}$, the increase of ultimate bearing capacity is 20.1%. It is only 1.1% higher than the E_{SCSC_zone} value is $1.3E_{Non\text{-}SCSC\_zone}$. This is because when the soil modulus around the pile exceeds a certain value, the increase of the soil modulus around the pile has little effect on the horizontal bearing capacity.

3.3. Bending Moment of the CCFSTP. Figure 16 shows the change rule of the bending moment of the CCFSTP with L_{SC}.

It can be seen from the Figure 16 that at the same depth, with the increase of steel casing length, the maximum bending moment of CCFSTP increases gradually. For both the RCP and the CCFSTP with an L_{SC} of 8 cm, the bending moment first increased and then decreased along the length direction as the depth increased. In addition, the bending moment started to sharply decrease at a certain depth and is negative after reaching zero, and it eventually became zero. This indicates that when the steel casing length is 8 cm, a pile undergoes inflection deformation along the length direction at a certain depth. Moreover, when the steel casing length is greater than 12 cm, the bending moment of the pile increases first and then decreases along the length direction and then decreases sharply at a certain depth, but it does not become negative as the depth continues to increase. As the steel casing length increases, the location of the cross-section of a pile at which its maximum bending moment occurs moves downward. The main reason is similar to the analysis in Section 3.1: with the increase of the length of the steel casing, the extrusion area of the steel casing increases and the pile-side soil resistance increases. In addition, as the length of the

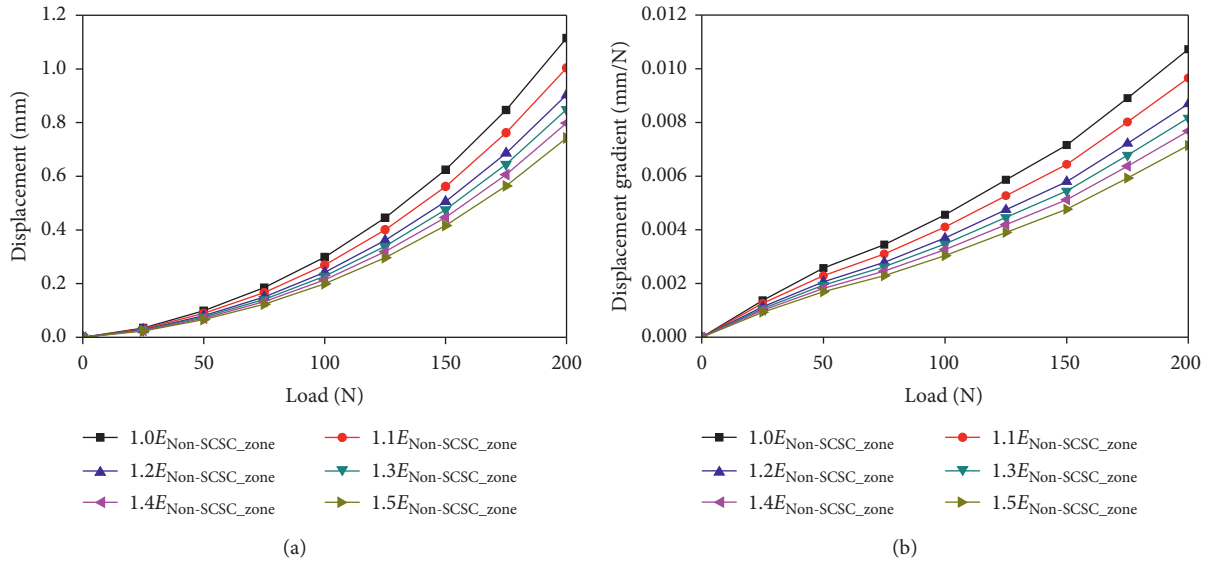

Figure 14: Load-displacement curves and load-displacement gradient curves of the CCFSTP under various $E_{\text{SCSC\_zone}}$ values.

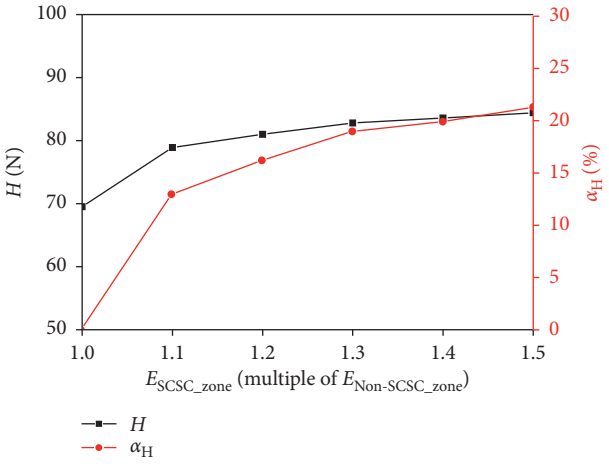

Figure 15: Effects of $E_{\text{SCSC\_zone}}$ on the ultimate horizontal bearing capacity of the CCFSTP.

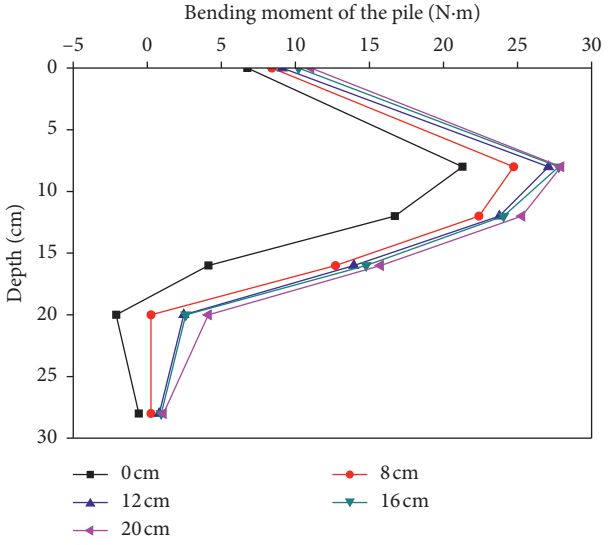

Figure 16: Change rule of the bending moment of the CCFSTP with L_{SC}.

steel casing increases, the stiffness of the CCFSTP increases, so the position where the maximum bending moment occurs moves down.

Figure 17 shows the change rule of the maximum bending moment of the CCFSTP and the location of the cross-section of the CCFSTP at which its maximum bending moment occurred as L_{SC} increased.

As shown in Figure 17, the maximum bending moment of the CCFSTP increases as the steel casing length increases. The maximum bending moment of the CCFSTP is 24.7 N·m, 27.1 N·m, 27.8 N·m, and 28.0 N·m when the steel casing length is 8 cm, 12 cm, 16 cm, and 20 cm, respectively, which are 16.5%, 27.8%, 31.1.5%, and 32.1% higher than that of the ordinary RCP. Evidently, when the steel casing length is less than 12 cm, the steel casing length relatively significantly affects the maximum bending moment of the CCFSTP; the effects of the steel casing length on the maximum bending moment of the CCFSTP decrease as the steel casing length increases beyond 12 cm. As the steel casing length increases, the location of the cross-section of the CCFSTP at which its maximum bending moment occurs moves slowly downward. This suggests that the location of the cross-section of the CCFSTP at which its maximum bending moment occurs is insignificantly affected by the steel casing length after the steel casing length reaches a certain value. This is because when the steel casing length exceeds a certain value, the increase of the steel casing length has little effect on the maximum bending moment of the CCFSTP.

Figure 18 shows the change rule of the bending moment of the CCFSTP with the $E_{\text{SCSC\_zone}}$.

Similar patterns can be observed in Figure 18 for the variations in the bending moment of the CCFSTP and the ordinary RCP along the length direction. The bending

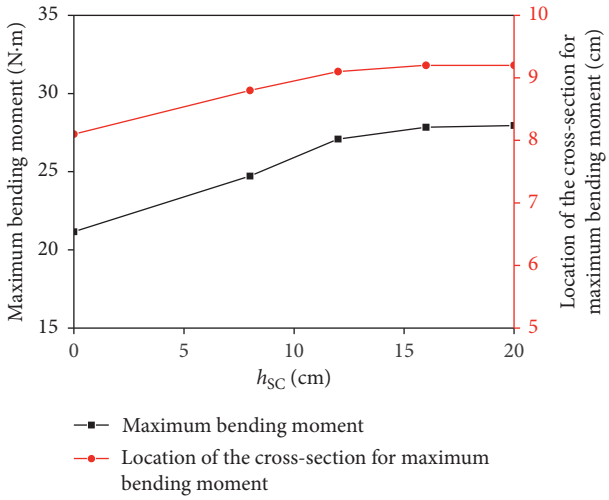

Figure 17: Change rule of the maximum bending moment of the CCFSTP and the location of the cross-section of the CCFSTP.

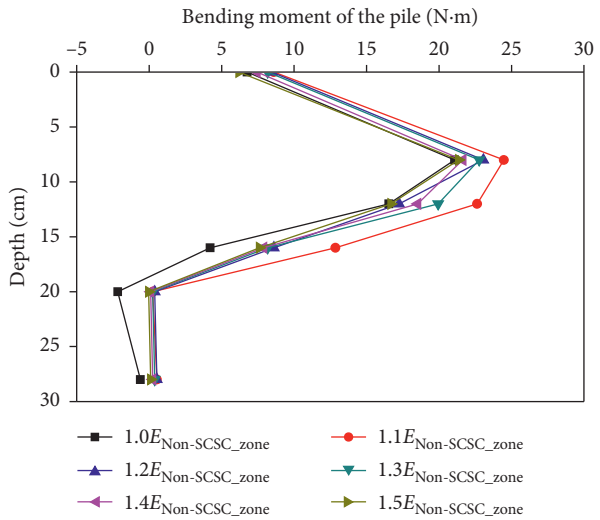

Figure 18: Change rule of the bending moment of the CCFSTP with E_{SCSC_zone}.

moment increases first, then decreases, and starts to decrease sharply at a certain depth; it becomes negative after reaching zero and eventually decreases to zero. The bending moment of the CCFSTP is greater than that of the ordinary RCP at the same cross-section. For the CCFSTP, with the same length of steel casing, its maximum bending moment gradually decreased as modulus of soil mass in the steel casing soil compaction zone increased. The main reason is that with the increase of modulus of soil mass in the zone, the soil around CCFSTP is not easy to be compressed and the pile-side soil resistance increases. Figure 19 shows the change rule of the maximum bending moment of the CCFSTP and the location of the cross-section of the CCFSTP at which the maximum bending moment occurred with increasing E_{SCSC_zone}.

As E_{SCSC_zone} values increases, the maximum bending moment of the CCFSTP decreases, but it remains greater than that of the ordinary RCP. The maximum bending

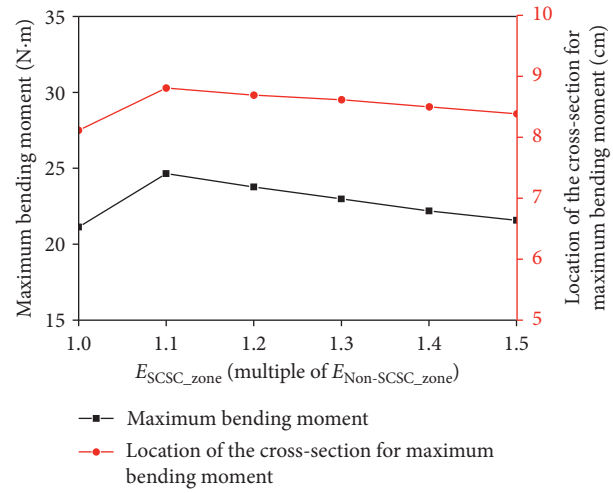

Figure 19: Change rule of the maximum bending moment of the CCFSTP and the location of the cross-section of the CCFSTP at which the maximum bending moment occurred.

moment of the CCFSTP is 24.7 N·m, 23.8 N·m, 23.0 N·m, 22.2 N·m, and 21.6 N·m when the modulus of soil mass in the steel casing soil compaction zone is $1.1E_{Non\text{-}SCSC\_zone}$, $1.2E_{Non\text{-}SCSC\_zone}$, $1.3E_{Non\text{-}SCSC\_zone}$, $1.4E_{Non\text{-}SCSC\_zone}$, and $1.5E_{Non\text{-}SCSC\_zone}$, respectively, which are 16.5%, 12.3%, 8.5%, 4.7%, and 1.9% higher than that of the ordinary RCP, respectively. Moreover, as E_{SCSC_zone} increases, the location of the cross-section of the CCFSTP at which its maximum bending moment occurs moves upward. However, due to the presence of the steel casing, the location of the maximum bending moment remains below the location of the cross-section of the ordinary RCP at which its maximum bending moment occurs. This suggests that changes in E_{SCSC_zone} have no significant effects on the location of the cross-section of the CCFSTP where its maximum bending moment occurs. This is mainly because when the modulus of soil mass in the steel casing soil compaction zone exceeds a certain value, it is difficult for the soil around the CCFSTP to continue to be compressed, and the increase of soil modulus has little effect on the maximum bending moment of CCFSTP.

3.4. Calculation of Optimal Reinforcement for CCFSTPs and Its Validation Based on an Engineering Structure. The above analysis shows that the bending resistance of the CCFSTP is higher than that of the ordinary RCP. However, in pile foundation design, the effects of the steel casing on the pile bending resistance are not taken into consideration; instead, the steel casing is only considered as a safety margin, which is evidently unreasonable. Therefore, it is necessary to analyze optimal reinforcement design for CCFSTPs.

For an ordinary RCP—a circular eccentric compression member with uniform circumferential reinforcement—when the number of longitudinal reinforcement is no less than six, the longitudinal reinforcement can be converted to an equivalent steel ring with a total area of $\sum_{i=1}^{n} A_{si}$ (A_{si} is the cross-sectional area of a single longitudinal reinforcement

and n is the number of longitudinal reinforcement) and a radius of r_s [31].

Let us set r as the cross-sectional radius of a pile foundation (i.e., the design radius) and r_s as the distance between the centre of the wall thickness of the equivalent steel ring and the centre of the cross-section (the same as the distance between the centre of the longitudinal reinforcement and the centre of the cross-section). Then, the thickness t_{s1} of the steel ring equivalent to the longitudinal reinforcement is

$$t_{s1} = \frac{\sum_{i=1}^{n} A_{si}}{2\pi r_s} = \frac{\sum_{i=1}^{n} A_{si}}{\pi r^2} \cdot \frac{r}{2\alpha} = \frac{\zeta r}{2\alpha}, \tag{2}$$

where ζ is longitudinal reinforcement ratio ($\zeta = \sum_{i=1}^{n} A_{si}/\pi r^2$) and$\alpha$ is ratio of the radius of the equivalent steel ring to the design radius of the pile foundation ($\alpha = r_s/r$).

Similar to the calculation of the bending resistance by converting the longitudinal reinforcement to an equivalent steel ring, the steel casing in the CCFSTP can also be converted to an equivalent steel ring with a radius of r_s at the same location as the longitudinal reinforcement based on the equivalence principle of cross-sectional bending resistance. In this way, the steel casing and the longitudinal reinforcement can be both included in the calculation of the bending resistance of the pile foundation, which will provide a basis for optimal reinforcement design for CCFSTPs. Figure 20 shows the method for converting the steel casing to an equivalent steel ring.

Based on the principle that the cross-sectional bending resistance of the steel casing equals that of the equivalent steel ring, we have

$$E_1 I_1 = E_2 I_2, \tag{3}$$

where E_1 and E_2 are elastic moduli of the steel casing and the longitudinal reinforcement, respectively (Pa) and I_1 and I_2 are moments of inertia of the steel casing and the longitudinal reinforcement relative to the centre of the cross-section, respectively (m^4).

For each steel casing and the equivalent steel ring, the wall thicknesses are far smaller than the distance between its centre and the centre of the cross-section ($t_s \ll r', t_{s2} \ll r_s$). Thus,

$$I_1 = \pi r'^3 t_s, I_2 = \pi r_s^3 t_{s2}, \tag{4}$$

where r' is distance between the centre of the wall thickness of the steel casing and the centre of the cross-section (m), r_s is distance between the centre of the wall thickness of the equivalent steel ring and the centre of the cross-section (m), t_s is wall thickness of the steel casing (m), and t_{s2} is wall thickness of the steel ring equivalent to the steel casing (m).

By substituting equation (4) into equation (3), we have

$$t_{s2} = \frac{E_1 r'^3}{E_2 r_s^3} \cdot t_s = \frac{E_1}{E_2 \alpha'^3} \cdot t_s, \tag{5}$$

where α' is ratio of the radius of the equivalent steel ring to the radius of the steel casing ($\alpha' = r_s/r'$).

$$n' = \frac{A_s}{A_{si}} = \frac{2\pi r_s t_{s2}}{A_{si}} = \frac{2E_1 r'^3 t_s}{E_2 r_0^2 r_s^2}, \tag{6}$$

where n' is the number of longitudinal reinforcement equivalent to the steel casing, A_s is the cross-sectional area of the steel ring equivalent to the steel casing (m^2), r_0 is the radius of the longitudinal reinforcement (m), and the remaining parameters have the same meaning as previously described.

As demonstrated in equation (6), in the bearing structure system of a CCFSTP, a steel casing with an elastic modulus of E_1, a wall thickness of t_s, and a radius of r' play the same role as n' number of longitudinal reinforcement with an elastic modulus of E_2 and a radius of r_0. On this basis, longitudinal reinforcement can be reasonably optimized for pile foundations.

3.5. A Case Study. CCFSTPs are widely used as the bridge foundations of Guangzhou-Jiangmen Expressway. A case study is performed with the FY3#-0 pile foundation of the Fuzhouhe Bridge in the Jiangnan segment of the TJ05 section of the Guangzhou-Jiangmen Expressway. The FY3#-0 CCFSTP contains longitudinal rebars of the same type and diameter but with three different lengths along the length of the pile (see Table 7).

The CCFSTP remains in a water environment for an extended period of time, and consequently, its steel casing is corroded to some extent. Therefore, the effects of corrosion on the steel casing need to be considered. According to the Specification for Pile Foundations of Harbor Engineering [32] and Specification for Design of Highways Reinforced Concrete and Prestressed Concrete Bridges and Culverts [33], a corrosion rate of 0.03 mm/year can be used for steel structures in river ports. Based on a design service life of 100 years, a thickness of 3 mm is included in the steel casing as a safety margin against corrosion. Thus, when calculating the horizontal bending resistance of the pile foundation, the contribution of this 3mm thickness of the steel casing should be deducted.

Based on equation (6), the number of longitudinal rebars equivalent to the steel casing in the pile foundation can be calculated. By substituting $E_1 = 2.05 \times 10^5$ MPa, $E_2 = 2 \times 10^5$ MPa, $r' = 0.9$ m, $r_s = 0.64$ m, $r_0 = 0.0125$ m, and $t_s = 0.007$ m into equation (6), we obtain

$$n' = \frac{2 \times 2.05 \times 10^5 \times 0.9^3 \times 0.007}{2 \times 10^5 \times 0.0125^2 \times 0.64^2} = 163.5. \tag{7}$$

Based on the above calculation, the bending resistance of the FY3#-0 CCFSTP provided by the built-in steel casing is equivalent to that provided by 163 longitudinal rebars with a diameter of 25 mm. This indicates that the steel casing can provide sufficient bending resistance to the pile foundation. Therefore, structural reinforcement should be designed for the CCFSTP with a minimum reinforcement ratio of 0.5% according to the Design Specification for Reinforced Concrete for Highways and Prestressed Concrete Bridges and Culverts while ensuring that the steel casing has a sufficient effective wall thickness [33].

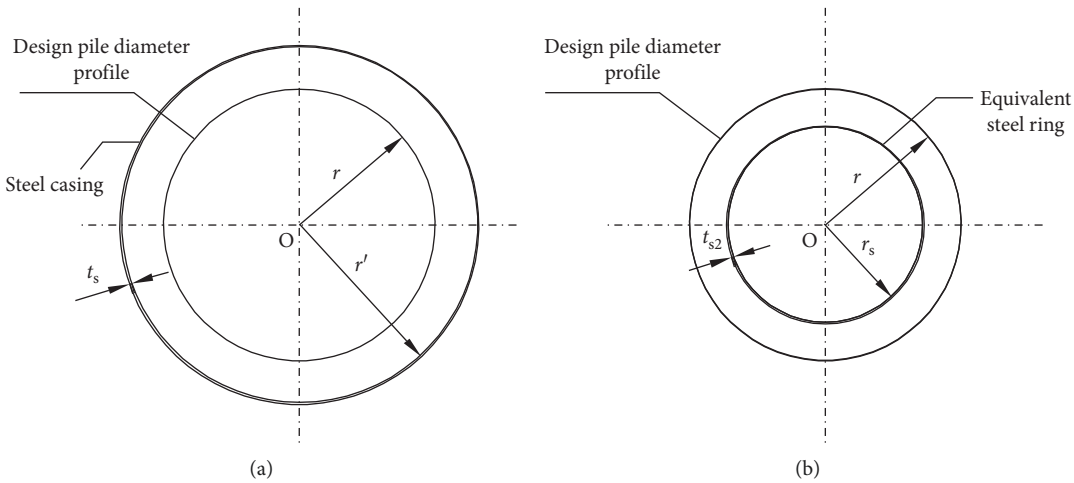

Figure 20: (a) Placement of the steel casing. (b) Equivalent steel ring.

Table 7: Reinforcement parameters of the FY3#-0 CCFSTP.

Pile length (cm)	Pile diameter (m)	Number of rebars	Number	Diameter (mm)	Length (cm)	Number of rebars	Total length (m)
6300	1.5	4	1	25	6419.7	7	449.4
			2	25	3624.3	8	289.9
			3	25	2624.3	15	393.6

Table 8: Parameters used in the calculation of optimal reinforcement for the FY3#-0 CCFSTP.

Elastic modulus of the steel casing E_1 ($\times 10^5$ MPa)	Elastic modulus of the rebars E_2 ($\times 10^5$ MPa)	Radius of the steel casing r' (cm)	Effective wall thickness of the steel casing t (mm)	Radius of the rebars r_0 (mm)	Radius of the equivalent steel ring r_s (cm)
2.05	2	90	7	12.5	64

The FY3#-0 has a diameter D of 1.5 m. For a structural reinforcement design based on a minimum reinforcement ratio of 0.5%, the number of the aforementioned longitudinal rebars required is

$$n = \frac{A\rho}{A_{si}} = \frac{\pi r^2 \rho}{\pi r_0^2} = \frac{3.14 \times 0.75^2 \times 0.005}{3.14 \times 0.0125^2} = 18. \quad (8)$$

Considering that the steel casing is mainly located in the upper section of the pile foundation, a reinforcement optimization principle that reduces the number of relatively short longitudinal rebars should be used. Based on the actual reinforcement in the FY3#-0 CCFSTP (Table 8), it is determined that only the No. 3 rebars in the original design need to be optimized. Eventually, 12 No. 3 rebars are removed. As a result, rebars with a total length of 314.9 m have been saved.

4. Conclusions

The ultimate horizontal bearing capacity of the CCFSTP is, to some extent, higher than that of an ordinary RCP. The longer the steel casing, the lower the maximum pile-side soil resistance. As the modulus of soil mass in the steel casing soil compaction zone increases, the maximum pile-side soil resistance increases. When the pile-side soil mass is relatively soft, increasing the steel casing length can compensate for the deficiency in the pile-side soil resistance. The maximum bending moment of the CCFSTP is greater than that of an ordinary RCP. The longer the steel casing, the greater the maximum bending moment of the CCFSTP and the lower the location of the cross-section of the CCFSTP at which the maximum bending moment occurs. The greater the E_{SCSC_zone} value, the smaller the maximum bending moment of the CCFSTP and the higher the location of the cross-section of the CCFSTP at which the maximum bending moment occurs.

A longitudinal reinforcement optimization equation for CCFSTPs is obtained based on a theoretical derivation, which provides theoretical guidance for the reasonable reinforcement of pile foundations. Due to the presence of a steel casing, a CCFSTP has excessive bending resistance. To save on the project investment, optimal reinforcement could be designed by using the reinforcement optimization equation for piles to reduce the number of longitudinal bars inside the pile while ensuring sufficient bending resistance of the pile.

Data Availability

The data used to support the findings of this study are included within the article.

Conflicts of Interest

The authors declare that there are no conflicts of interests regarding the publication of this paper.

Acknowledgments

The study was supported by the Key Transportation Science and Technology Program of Guangdong Province under Grant no. 2011-01-001. The authors would also like to express their great appreciation to Chenxin Xi for helping in the development of the experiments and to Hangzhou Su for refining and finalising the manuscript.

References

[1] Z. Feng, H. Hu, Y. Dong et al., "Effect of steel casing on vertical bearing characteristics of steel tube-reinforced concrete piles in loess area," *Applied Sciences*, vol. 9, no. 14, p. 2874, 2019.

[2] J. X. Lai, H. Q. Liu, J. L. Qiu, and J. X. Chen, "Settlement analysis of saturated tailings dam treated by CFG pile composite foundation," *Advances in Materials Science and Engineering*, vol. 10, 2016.

[3] J. Lai, H. Liu, J. Qiu et al., "Settlement analysis of saturated tailings dam treated by CFG pile composite foundation," *Advances in Materials Science and Engineering*, vol. 2016, pp. 1–10, 2016.

[4] Q.-Q. Zhang, L.-P. Li, and Y.-J. Chen, "Analysis of compression pile response using a softening model, a hyperbolic model of skin friction, and a bilinear model of end resistance," *Journal of Engineering Mechanics*, vol. 140, no. 1, pp. 102–111, 2014.

[5] Q.-Q. Zhang, S.-W. Liu, S.-M. Zhang, J. Zhang, and K. Wang, "Simplified non-linear approaches for response of a single pile and pile groups considering progressive deformation of pile-soil system," *Soils and Foundations*, vol. 56, no. 3, pp. 473–484, 2016.

[6] Q.-Q. Zhang and Z.-M. Zhang, "A simplified nonlinear approach for single pile settlement analysis," *Canadian Geotechnical Journal*, vol. 49, no. 11, pp. 1256–1266, 2012.

[7] Y. Dong, Z. Feng, J. He, H. Chen, G. Jiang, and H. Yin, "Seismic response of a bridge pile foundation during a shaking table test," *Shock and Vibration*, vol. 2019, Article ID 9726013, 16 pages, 2019.

[8] J. Wang, W. Li, and Z. Song, "Development and implementation of new triangular finite element based on MGE theory for bi-material analysis," *Results in Physics*, vol. 13, Article ID 102231, 2019.

[9] X. Tian, Z. Song, and J. Wang, "Study on the propagation law of tunnel blasting vibration in stratum and blasting vibration reduction technology," *Soil Dynamics and Earthquake Engineering*, vol. 126, Article ID 105813, 2019.

[10] Z. Feng, H. Hu, R. Zhao et al., "Experiments on reducing negative skin friction of piles," *Advances in Civil Engineering*, vol. 10, 2019.

[11] Ministry of Housing and Urban-Rural Development of the People's Republic of China, *Technical Specification for Concrete Filled Steel Tubular Structures, (GB 50936-2014)*, China Architecture & Building Press, Beijing, China, 2014.

[12] American Institute of Steel Construction (AISC), *Specification for Structural Steel Buildings, (ANSI/AISC 360-16)*, American Institute of Steel Construction (AISC), Chicago, IL, USA, 2016.

[13] Architectural Institute of Japan (AIJ), *Recommendations for Design and Filled Steel Tubular Structures*, Architectural Institute of Japan, Tokyo, Japan, 2008.

[14] British Standards Institution, *Steel, Concrete and Composite Bridges, Part 5: Code of Practice for Design of Composite Bridges, (BS5400-5)*, British Standards Institution, London, UK, 2005.

[15] British Standards Institution, *Design of Composite Steel and Concrete Structures, (Eurocode 4)*, British Standards Institution, London, UK, 2007.

[16] M. Johansson and K. Gylltoft, "Mechanical behavior of circular steel-concrete composite stub columns," *Journal of Structural Engineering*, vol. 128, no. 8, pp. 1073–1081, 2002.

[17] F. Trentadue, G. Quaranta, and G. C. Marano, "Closed-form approximations of interaction diagrams for assessment and design of reinforced concrete columns and concrete-filled steel tubes with circular cross-section," *Engineering Structures*, vol. 127, pp. 594–601, 2016.

[18] M. Yousuf, B. Uy, Z. Tao, A. Remennikov, and J. Y. R. Liew, "Transverse impact resistance of hollow and concrete filled stainless steel columns," *Journal of Constructional Steel Research*, vol. 82, no. 82, pp. 177–189, 2013.

[19] V. I. Patel, Q. Q. Liang, and M. N. S. Hadi, "Biaxially loaded high-strength concrete-filled steel tubular slender beam-columns, part II: parametric study," *Journal of Constructional Steel Research*, vol. 110, no. 75, pp. 200–207, 2015.

[20] V. I. Patel, Q. Q. Liang, and M. N. S. Hadi, "Nonlinear analysis of axially loaded circular concrete-filled stainless steel tubular short columns," *Journal of Constructional Steel Research*, vol. 101, no. 101, pp. 9–18, 2014.

[21] N. K. Brown, M. J. Kowalsky, and J. M. Nau, "Impact of D/t on seismic behavior of reinforced concrete filled steel tubes," *Journal of Constructional Steel Research*, vol. 107, pp. 111–123, 2015.

[22] D. A. Aguirre, M. J. Kowalsky, J. M. Nau, M. Gabr, and G. Lucier, "Seismic performance of reinforced concrete filled steel tube drilled shafts with inground plastic hinges," *Engineering Structures*, vol. 165, 2018.

[23] L. A. Montejo, L. A. González-Román, and M. J. Kowalsky, "Seismic performance evaluation of reinforced concrete-filled steel tube pile/column bridge bents," *Journal of Earthquake Engineering*, vol. 16, no. 3, pp. 401–424, 2012.

[24] E.-b. Jung, S.-H. Lee, J.-H. Yoo, C. Roeder, and D. Lehman, "Shear behavior of large-diameter concrete filled tube (CFT)," *International Journal of Steel Structures*, vol. 17, no. 4, pp. 1651–1665, 2017.

[25] G. F. Du, M. Babic, F. H. Wu, X. Zeng, and X. M. Bie, "Experimental and numerical studies on concrete filled circular steel tubular (CFCST) members under impact loads," *International Journal of Civil Engineering*, vol. 3, pp. 1–16, 2018.

[26] X. Ding, Y. Fan, P. Li, and G. Kong, "Vertical dynamic response of a concrete filled steel tube due to transient impact load: analytical solution," *International Journal of Structural Stability and Dynamics*, vol. 16, no. 1, Article ID 1640014, 2016.

[27] A.-Z. Zhu, W. Xu, K. Gao, H.-B. Ge, and J.-H. Zhu, "Lateral impact response of rectangular hollow and partially concrete-filled steel tubular columns," *Thin-Walled Structures*, vol. 130, pp. 114–131, 2018.

[28] C. Wang, X. Liu, and P. Li, "Experimental behavior of concrete-filled steel tubular members subjected to lateral loads,"

Advances in Materials Science and Engineering, vol. 2018, Article ID 9065378, 15 pages, 2018.

[29] National Energy Administration, *Specification for Geotechnical Centrifuge Model Test Techniques, (DL/T 5102-2013)*, China Electric Power Press, Beijing, China, 2013.

[30] X. N. Gong, *Handbook for Pile Foundation Engineering*, China Architecture & Building Press, Beijing, China, 2016.

[31] Z. Fang, "Strength and deformation of R. C. eccentrically compressive members with circular section," *China Journal of Highway & Transport*, vol. 7, no. 1, pp. 55–58, 1994.

[32] Ministry of Transport of the People's Republic of China, *Specification for Pile Foundations of Harbor Engineering, (JTS 167-4-2012)*, China Communications Press, Beijing, China, 2012.

[33] Ministry of Transport of the People's Republic of China, *Specification for Design of Highways Reinforced Concrete and Prestressed Concrete Bridges and Culverts, (JTG D62-2012)*, China Communications Press, Beijing, China, 2012.